AIMS Mathematics, 10(5): 12554–12575.
DOI:10.3934/math.2025566
Received: 28 January 2025
Revised: 05 May 2025
Accepted: 20 May 2025
Published: 29 May 2025

https://www.aimspress.com/journal/Math

Research article

Dynamic analysis and multistability of a discontinuous Jerk-like system

Thoraya N. Alharthi*

Department of Mathematics, College of Science, University of Bisha, P. O. Box 551, Bisha 61922, Saudi Arabia

* **Correspondence:** Email: talhrthe@ub.edu.sa.

Abstract: This paper introduces a novel Jerk-like system characterized by discontinuous vector fields along a codimension-1 switching surface. This system is capable of exhibiting both the existence and non-existence of equilibria in response to defined arbitrary functions. Non-smooth properties are investigated, which are essential for identifying and allowing rapid transient responses to dynamic events that influence the system's behaviors. The proposed discontinuous systems, which include both crossing and sliding solutions, are examined specifically for the detection of self-excited and hidden attractors. The dynamic characteristics of these systems are examined utilising the criteria for discontinuous solutions, the Poincarè return map, the spectrum of Lyapunov exponents, and bifurcation diagrams. The analysis reveals that incorporating the switching surface into Jerk-like subsystems alters the dimensions of the generated attractors. This alteration provides the necessary basis for the formation of period-doubling orbits that culminate in chaotic attractors. In the scenarios involving sliding motion within the proposed system, various attractors are identified that exhibit sensitive dependence not only on the initial conditions and parameter variations, but also on the interaction of the flow with the discontinuity surface. An interesting result indicates that the proposed novel Jerk system, which is distinguished by the absence of both real and virtual equilibria, reveals a family of periodic orbits in the sliding region surrounding the pseudo-equilibrium. The use of analytical solutions and numerical techniques successfully identifies a wide range of attractors, including periodic orbits, period-doubling phenomena, and chaotic behavior in both crossing and sliding modes.

Keywords: Jerk-like chaotic system; discontinuous systems; self-excited and hidden attractors; multistability; sliding motion
Mathematics Subject Classification: 34A36, 34D23, 34H10, 37G15

1. Introduction

Chaos theory has developed over decades, especially in nonlinear dynamical systems, since its discovery by [1]. It has been applied in a variety of fields, such as disease control and prevention [2], mechanics [1, 3], biology [4], cryptography [5], secure communications [6], and other application areas. Various published works [7–9] have presented the concept of two different types of attractors in continuous nonlinear dynamic systems, particularly regarding the behavior and the emergence or disappearance of equilibrium (fixed) points. An attractor is called a self-excited attractor if it has a basin of attraction that is associated with an unstable equilibrium. Conversely, an attractor is called hidden if its basin of attraction does not intersect with a small neighborhood of any equilibrium point [10]. The presence of multiple attractors, known as multistability, is a common phenomenon observed in many scientific fields and in nature [11]. Generally, the convergence to one of these attractors depends solely on the initial conditions or a specific set of parameters. Bifurcation analysis tools, particularly bifurcation diagrams, are essential for investigating the multiple attractors and qualitative properties of nonlinear dynamical systems. A wide range of software applications have been developed to calculate and display bifurcations, such as MATCONT [12], AUTO-07p [13], and PyDSTool [14]. In this context, the authors of [15] presented an advanced algorithm and specialized software for plotting bifurcation diagrams, which used graphics processing units (GPUS) accelerated computations in conjunction with a highly efficient semi-implicit ordinary differential equation (ODE) solver.

Hidden attractors have recently emerged as an important topic in a variety of theoretical and applied areas of continuous dynamic systems. These attractors can be identified within dynamic systems, categorized into the following four types: dynamic systems with no equilibrium points [16–18], systems that only have steady equilibrium points [19, 20], systems with an infinite number of equilibrium points [21], systems with coexisting self-excited attractors [22].

The Jerk system has emerged as one of the chaotic systems that have recently attracted significant interest. Many researchers have studied the Jerk system in the presence of continuous behavior [23], where some researchers have looked at the Jerk-like system in the presence of discontinuous behavior [24]. Other authors [25, 26], have directed their attention towards exploring the presence of periodic orbits, multistability, and the coexistence of attractors within specific parameter regions. Futhermore, [22] has demonstrated that both versions of the Jerk system exhibit multistability, where different types of attractors, such as periodic, chaotic, or a combination of both, can exist together in the phasespace, regardless of whether they are self-excited or hidden. Recently, the authors of [27] highlighted the presence of both single- and dual-scroll expansions in the three-dimensional (3D) and four-dimensional (4D) Jerk systems.

Moreover, there have been a few studies that examined the Jerk system in the presence of discontinuous behavior. Linz and Sprott [28] developed a comprehensive range of piecewise-linear Jerk functions. The dependence of these systems is exclusively on the switching between two vectors, dictated by the sign of one variable, thereby inhibiting the occurrence of a sliding mode. Hosham [24] proposed a novel chaotic Jerk system that is defined across four distinct domains designated by codimension-2 discontinuity surfaces, and it has been discovered that the chaotic behavior can exhibit a segment of sliding motion. In general, the existence of discontinuous behavior is responsible for the complex phenomena observed in real systems [29, 30], particularly in ecological contexts with epidemic models [31].

This study is motivated by the desire to propose and analyze a nonlinear Jerk-like system with discontinuous behavior, with a particular emphasis on the detection of hidden and self-excited attractors. One advantage of the proposed system is its ability to reveal the existence and absence of equilibrium points on the basis of defined arbitrary functions. We explore nonsmooth properties because they are critical for identifying and facilitating rapid transient responses to dynamic events that influence a system's behaviors. To obtain periodic orbits numerically, a system of nonlinear algebraic equations needs to be set up, based on analytical solutions. A variety of Jerk-like system classes, including both crossing and sliding solutions, are investigated with the goal of detecting self-excited and hidden attractors. To examine the dynamic properties of these systems, various tools are used, including analytical criteria for discontinuous solutions, the Poincarè return map, the spectrum of Lyapunov exponents, and bifurcation diagrams.

The novelty of this work compared with prior studies [16, 23, 32] is summarized as follows.

- We present a novel Jerk system that incorporates discontinuities, enabling the exhibition of both sliding and crossing modes. This highlights the unique contribution and significance of the present work in advancing the study of discontinuous Jerk systems.
- Flexibility in equilibrium behavior is shown, where the proposed systems may (or may not) exhibit equilibrium points on one or both sides of the discontinuity surface.
- A novel and interesting result is the discovery of a periodic orbit completely limited to the sliding mode, which is an uncommon and noteworthy phenomenon in the study of discontinuous Jerk systems.

The structure of this paper is as follows: Section 2 introduces the proposed discontinuous Jerk-like system and investigates its nonsmooth properties, focusing on the fundamental principles governing flow interactions on a codimension-1 switching surface. Section 3 includes a theoretical analysis as well as numerical simulations of various classes of Jerk-like systems. This includes examining crossing solutions in order to identify self-excited and hidden attractors. Section 4 presents hidden attractors with a sliding mode. Finally, the conclusion of this paper is given in Section 5.

2. Discontinuous Jerk-like system

In physics, a Jerk equation takes the general form

$$\dddot{x} = \mathbb{J}(x, \dot{x}, \ddot{x}), \tag{2.1}$$

where $\mathbb{J}$ is a smooth function in R^3, and the term "Jerk" refers to the definition of successive derivatives in mechanical systems. Moreover, x, $\dot{x}$, $\ddot{x}$, and $\dddot{x}$ are the displacement, velocity, acceleration, and Jerk, respectively. Jerk systems are frequently considered to be the simplest sort of chaotic systems [26] and possess several applications in scientific and engineering fields [32]. The most commonly reported Jerk systems use quadratic, cubic, exponential, and hyperbolic nonlinearities, and they attempt to design and implement circuits for these systems [33]. Jerk systems with some type of discontinuity have recently gained substantial interest and have been extensively reported in the pertinent literature because of their simplicity and complex dynamics; see, for instance, [24].

In our research, we analyze Jerk-like systems, which are described by piecewise differential systems

composed of two differential systems separated by a switching surface $\hbar(x, \dot{x}, \ddot{x}) = 0$, as follows:

$$\dddot{x} = \begin{cases} \mathbb{J}_a(x, \dot{x}, \ddot{x}), & \hbar(x, \dot{x}, \ddot{x}) < 0; \\ \mathbb{J}_b(x, \dot{x}, \ddot{x}), & \hbar(x, \dot{x}, \ddot{x}) > 0. \end{cases} \tag{2.2}$$

The motivation for this work is to study the discontinuous behavior of the nonlinear Jerk-like system above in the presence of hidden and self-excited attractors. Recent research on discontinuous dynamic systems, as presented in [34], demonstrates that a planar linear nonsmooth system devoid of equilibria in each subsystem, whether real or virtual, can nonetheless display a minimum of one limit cycle. In our recent study [35], the hidden dynamics of the proposed three-dimensional discontinuous system are related to the fact that only one subsystem in the whole system lacks an equilibrium point. The investigation of the dynamics and bifurcations of the discontinuous system (2.2) has significantly increased, as researchers have come to understand that discontinuous systems can exhibit a diverse range of complicated dynamic phenomena that require attention in their applications. The grazing bifurcation framework for closed orbits [10], which includes the collision of closed orbits with the switching manifold, has been thoroughly explained and applied in systems containing dry friction and mechanical impact oscillators [36]. In general, bifurcations in discontinuous systems are categorized into two types: nonstandard bifurcations, which are unique to discontinuous systems such as sliding bifurcation or discontinuity-induced bifurcations, and standard bifurcations, which are identical to those found in continuous systems such as saddle-node and Hopf bifurcations.

The equation $\hbar(x, \dot{x}, \ddot{x}) = 0$ is considered to establish a surface of two dimensions, known as the switching manifold, which is indicated by $\mathbb{D}$. The system (2.2) is written as a 3D first-order differential equation as follows:

$$\dot{\eta} = \begin{cases} \mathbb{J}_a(\eta), & \hbar(\eta) < 0, \\ \mathbb{J}_b(\eta), & \hbar(\eta) > 0, \end{cases} \tag{2.3}$$

where $\eta =< x, \dot{x}, \ddot{x} >$ is a vector in a 3D space.

Assume that $\mathbb{U} \subset \mathbb{R}^3$ is open, $\hbar(\eta) : \mathbb{U} \to \mathbb{R}^d$, $\eta \in \mathbb{R}^3$, and $d \leqslant 3$ is a continuously differentiable function with a regular value of 0. To ensure there is only a codimension-1 discontinuity manifold, assume that the gradient vector $\nabla\hbar(\eta)$ does not vanish in any part of $\mathbb{D}$. If $\hbar(\eta) = \dot{\hbar}(\eta) = ... = \hbar^{r-1}(\eta) = 0$, then the motion of (2.2) is called an r-sliding mode; for example, see [37]. Let $\sigma_a = (\nabla\hbar(\eta))^T \mathbb{J}_a(\eta)$ and $\sigma_b = (\nabla\hbar(\eta))^T \mathbb{J}_b(\eta)$, where the elements of $\mathbb{J}_a(\eta)$ and $\mathbb{J}_b(\eta)$ are oriented towards $\nabla\hbar(\eta)$.

2.1. Nonsmoothness properties

When a trajectory intersects with a discontinuity surface, the system's dynamics cannot be represented by a single continuous vector field. In other words, as the trajectory approaches a discontinuity surface, two options may arise: Cross the surface or stay on it. If we choose to stay on the surface, we must describe the motion that occurs there, specifically a sliding motion. Therefore, it becomes necessary to define additional rules to to characterize distinct potential behaviors.

Definition 1. *The partial region of* $\mathbb{D}$ *is known as [36]*

- A direct crossing zone $\mathbb{D}^c := \{\eta \in \mathbb{R}^3 \mid \sigma_a(\eta)\,\sigma_b(\eta) > 0\}$, which is divided into $\mathbb{D}_a^c := \{\eta \in \mathbb{R}^3 \mid \sigma_a(\eta) < 0, \sigma_b(\eta) < 0\}$, and $\mathbb{D}_b^c := \{\eta \in \mathbb{R}^3 \mid \sigma_a(\eta) > 0,\ \sigma_b(\eta) > 0\}$;
- An attracting sliding zone $\mathbb{D}_a^s := \{\eta \in \mathbb{R}^3 \mid \sigma_a(\eta) > 0, \text{ and } \sigma_b(\eta) < 0\}$;
- A repelling sliding zone $\mathbb{D}_r^s := \{\eta \in \mathbb{R}^3 \mid \sigma_a(\eta) < 0, \text{ and } \sigma_b(\eta) > 0\}$,

where $\mathbb{D} = \mathbb{D}^c \cup \mathbb{D}_a^s \cup \mathbb{D}_r^s$.

The transition between these modes highlights the complex dynamics inherent in the proposed nonsmooth Jerk system. When the orbit of (2.3) approaches an attracting sliding region, it may touch the sliding surface and proceed to slide along it. This behavior is characterized by the Fillipov extension [36, 38] as follows:

$$\dot{\eta} = F_s(\eta) = S_a(\eta)\mathbb{J}_a(\eta) + S_b(\eta)\mathbb{J}_b(\eta), \quad \eta \in \mathbb{D}, \tag{2.4}$$

where $S_a(\eta) = 1 - S_b(\eta)$, and $S_b(\eta) = \frac{\nabla\hbar(\eta)^T\mathbb{J}_b(\eta)}{\nabla\hbar(\eta)^T\left(\mathbb{J}_b(\eta) - \mathbb{J}_a(\eta)\right)}$. The borders of these regions are formed by the equations $\sigma_a(\eta_0) = 0$ and $\sigma_b(\eta_0) = 0$, where $\eta_0 \in \mathbb{D}$ are called the tangent points. This indicates that at any point of $\eta_0 \in \mathbb{D}$, the orbit of $\mathbb{J}_a$ and $\mathbb{J}_b$ typically exhibits a quadratic tangency with $\mathbb{D}$.

Definition 2. *The point* $\bar{\eta} \in \mathbb{R}^3$ *is an equilibrium point for the subsystem* $\dot{\eta} = \mathbb{J}_a(\eta) \quad [\dot{\eta} = \mathbb{J}_b(\eta)]$ *if* $\mathbb{J}_a(\bar{\eta}) = 0\ [\mathbb{J}_b(\bar{\eta}) = 0]$*), and it is termed [24]:*

- An admissible point if $\bar{\eta} \in \mathbb{D}_- \quad [\bar{\eta} \in \mathbb{D}_+]$;
- Virtual if $\bar{\eta} \in \mathbb{D}_+ \quad [\bar{\eta} \in \mathbb{D}_-]$;
- A boundary equilibrium if $\hbar(\bar{\eta}) = 0$.

In addition, the sliding flow (2.4) exhibits a pseudo-equilibrium point if $\hbar(\bar{\eta}) = F_s(\bar{\eta}) = 0$.

The bifurcation that emerges from these fixed points results in what is known as a discontinuous bifurcation, in which the generalized set-valued Jacobian is defined as follows:

$$D\mathbb{J}(\bar{\eta}) = (D\mathbb{J}_b(\bar{\eta}) - D\mathbb{J}_a(\bar{\eta}))\alpha + D\mathbb{J}_a(\bar{\eta}), \ \ 0 \leqslant \alpha \leqslant 1.$$

This formula describes the Jacobian's behavior at $\bar{\eta} \in \mathbb{D}$. The literature [36, 39] discussed discontinuous bifurcation and discontinuity-induced bifurcation in various examples.

Assume that $\tilde{\eta} \in \mathbb{D}_a^c$. The flow generated by $\dot{\eta} = \mathbb{J}_a(\eta)$ intersects $\mathbb{D}$ at time t_a, after which it continues according to the flow defined by $\dot{\eta} = \mathbb{J}_b(\eta, t_a)$, reaching $\mathbb{D}$ again at time t_b. Hence, the variational equations for the trajectories for the piecewise smooth system (2.3) are

$$\begin{cases} \dot{\eta} = \mathbb{J}_a(\eta), \quad \eta(0) = \tilde{\eta} : \dot{\mathbb{Y}}_a = \frac{\partial}{\partial\eta}\mathbb{J}_a(\tilde{\eta})\mathbb{Y}_a, \quad \mathbb{Y}_a(0) = I; \\ \dot{\eta} = \mathbb{J}_b(\eta), \quad \eta(0) = \tilde{\eta} : \dot{\mathbb{Y}}_b = \frac{\partial}{\partial\eta}\mathbb{J}_b(\tilde{\eta})\mathbb{Y}_b, \quad \mathbb{Y}_b(0) = I. \end{cases} \tag{2.5}$$

At the intersection point and time $(\bar{t}_a, \tilde{\eta})$, we have $\mathbb{Y}_b = \bar{\mathbb{S}}\mathbb{Y}_a$, where $\bar{\mathbb{S}}$ is called the jump or saltation matrix, defined as. $\bar{\mathbb{S}} = I + \frac{\left(\mathbb{J}_b(\bar{t}_a,\tilde{\eta}) - \mathbb{J}_a(\bar{t}_a,\tilde{\eta})\right)(\nabla\hbar(\tilde{\eta}))^T}{(\nabla\hbar(\tilde{\eta}))^T\mathbb{J}_a(\bar{t}_a,\tilde{\eta})}$; see [39]. These properties serve as valuable tools for addressing discontinuities and refine the flow trajectory on $\mathbb{D}$.

2.2. The proposed discontinuous systems

We consider the vector fields of (2.3) defined as follows:

$$\dot{\eta} = \begin{cases} \mathbb{J}_a(\eta) = \begin{pmatrix} y \\ z \\ -az - y^2 + G_a(\eta) \end{pmatrix}, & \hbar(\eta) < 0, \\ \mathbb{J}_b(\eta) = \begin{pmatrix} y \\ z \\ -az + y^2 + G_b(\eta) \end{pmatrix}, & \hbar(\eta) > 0, \end{cases} \tag{2.6}$$

where $a > 0$ and the phase space is divided into two domains $\mathbb{D}^{\pm} = \{X \in \mathbb{U} \mid \pm\hbar(\eta) > 0\}$ separated by a hyperplane $\mathbb{D} = \{X \in \mathbb{R}^3 \mid \hbar(\eta) = x = 0\}$, and $\eta = (x, y, z)^T$. Furthermore, this system has only the crossing mode and cannot exhibit the sliding mode due to $\mathbb{D}_s = \{\varnothing\}$. The divergence of the system (2.6) is calculated using the following formula:

$$\nabla\mathbb{J} = -a + \frac{\partial G_i}{\partial z}, \quad i = a, b.$$

The choice of the function G_i is then determined by whether or not both subsystems in (2.6) are dissipative. The functions $G_i(\eta)$ and $\hbar(\eta)$ are crucial in defining the behavior of the proposed discontinuous systems, leading to different dynamic scenarios such as direct crossing and sliding modes, as discussed below.

3. Theoretical analysis and numerical simulations

This section aims to investigate the diverse range of dynamic behaviors exhibited by the system (2.6) through the utilization of phase portraits, time-domain waveforms, Poincaré maps, Lyapunov exponents, and bifurcation diagrams.

The equilibrium points of the system (2.6) can be determined by solving the subsequent equations $\mathbb{J}_a(\eta) = 0$ and $\mathbb{J}_b(\eta) = 0$, and $\eta \in \mathbb{R}^3$.

Definition 3. *The subsystems described by* (2.6) *possess an equilibrium point denoted* $\bar{\eta}$ *if the conditions* $G_a(\bar{\eta}) = 0$ *and* $G_b(\bar{\eta}) = 0$ *are satisfied. Consequently, all resulting attractors are classified as self-excited. Otherwise, the subsystems* (2.6) *have no equilibrium point, and hence the resulting attractors are all hidden.*

3.1. Case I: $\bar{\eta} = \vec{0} \in \mathbb{D}$ *and* $G_a(\bar{\eta}) = G_b(\bar{\eta}) = 0$.

The unknown functions within the system described by (2.6) are defined as follows: $G_a(\eta) = G_b(\eta) = -x$. Consequently, the origin emerges as the unique equilibrium point of this system. Furthermore, the Jerk system (2.6) is rewritten as

$$\dot{\eta} = A\eta + \begin{cases} -y^2 e_3, & x < 0, \\ y^2 e_3, & x \geqslant 0, \end{cases} \tag{3.1}$$

where $e_3 \in R^3$ is the third basis vector of R^3, and the continuity property can be clearly identified, since the only variation between the two subsystems is found in the third row.

Therefore, at the point $\eta_0 \in \mathbb{D}$, only a direct crossing region $\mathbb{D}^c$ is present, as both subsystems reflect the same value. Unlike Filippov systems (2.4), the systems defined by Eq (3.1), in conjunction with the continuity condition, cannot exhibit sliding behavior on $\mathbb{D}$. Therefore, trajectories that approach $\mathbb{D}$ will cross it immediately. A coefficient matrix $A \in R^{3\times 3}$ is a matrix consisting of the coefficients of the variables in a set of linearized systems (3.1). The characteristic equation for these linearized systems is provided as a depressed cubic equation $\lambda^3 + a\lambda^2 + 1 = 0$. Since the discriminant, which is derived from the coefficients of this cubic equation, is negative, it implies that the cubic has a single real root $\lambda_1 = \mu \in \mathbb{R}$ and two complex conjugate roots $\lambda_{2,3} = \alpha \pm i\beta$, such that $\alpha = \frac{1}{2\mu^2} > 0$, and $\mu = -(a+2\alpha) = -1/(\alpha^2+\beta^2) < 0$ (i.e., the origin point is a saddle-focus point, indicating the potential of self-excited strange attractors). According to the Routh-Hurwitz criterion, the equilibrium point exhibits instability in both subsystems. Additionally, the Routh-Hurwitz criterion, which is derived from the Sturm series, provides the essential conditions for the occurrence of a Hopf bifurcation in the system (3.1).

Lemma 1. *The dynamic system described by* (3.1) *exhibits a Hopf bifurcation if* $a \to \infty$.

To prove the Lemma above, let us consider the Sturm series denoted by $S_i, i = 0, 1, 2, ..., k$, which is associated with a characteristic equation $\lambda^3 + a\lambda^2 + 1 = 0$. This sequence is generated using a recursive process that begins with the polynomial and its derivative. It is used to determine the number of real roots of the characteristic equation within a given interval by observing the sign variations throughout the sequence. The series S_i is defined as follows:

$$S_i(\sigma) = C_{i,0}\sigma^{k-i} + C_{i,1}\sigma^{k-i-2} + ...$$

where $C_{i,0}$ are indicative of what are termed Hurwitz determinants; for an in-depth discussion, see [40]. We find that the Hurwitz determinants $C_{0,0} = 1 > 0$, $C_{1,0} = a > 0$, and $C_{1,1} = -1 < 0$. In addition, condition $C_{2,0} = -\frac{1}{a}$ must approach zero to ensure that the roots of the characteristic equation possess negative real parts, with the exception of a purely imaginary conjugate pair, which arises as a approaches infinity.

The matrix A has a real eigenvalue μ associated with the eigenvector v_1 and a pair of complex conjugate eigenvalues $\alpha \pm i\beta$, which correspond to the eigenvectors $v_2 \mp iv_3$. The general solution of the linear system $\dot{\eta} = A\eta$ can be expressed as follows:

$$\eta(t) = e^{\mu t}\xi_1 + e^{\alpha t}\left(\xi_2\left(\cos(\beta t)v_2 + \sin(\beta t)v_3\right) + \xi_3\left(\cos(\beta t)v_3 - \sin(\beta t)v_2\right)\right), \tag{3.2}$$

where $\xi_i, i = 1, 2, 3$ are determined by the initial condition η_0. Since $\mu < 0$ and $\alpha > 0$, at $t \to \infty$, the term $e^{\mu t}$ governs a decay component, while $e^{\alpha t}$ governs a growth component, which modifies the oscillatory terms. The oscillations may cause periodic behavior.

The general solution of the system (3.1) can be described using an exponential matrix as follows:

$$\breve{\mathcal{P}}(\eta) = \exp(A\ t)\ \eta_0 \pm \int_0^t \exp(A(t-s))\ y(s)^2\ e_3\ \ ds, \ \text{ for } \ \pm e_1^T\eta_0 \geqslant 0, \tag{3.3}$$

where $e_i \in R^3, i = 1, 2, 3$; are the standard basis of a coordinate vector space. Note that the integration term in Eq (3.3) can be written explicitly; however, the resulting formulas are rather

complex. Consequently, the dynamics of the system (3.1) can be analyzed using a discrete Poincarè map $\check{\mathcal{P}}$, with the Poincarè section established at the hypersurface $\mathbb{D}$. Starting with the initial condition $\eta_0 \in \mathbb{D}^c_-$, the orbit that begins at η_0 at zero time will re-enter $\mathbb{D}^c_+$ after the duration $t = t_a(\eta)$, reaching the point $\eta_b = \eta(t_a) \in \mathbb{D}^c_+$. After the crossing event, the orbit continues to oscillate with the subsystem $\dot{\eta} = \mathbb{J}_b(\eta)$ until it reaches $\mathbb{D}^c_-$ again, following the return time $t_b(\eta)$ at the crossing point $\eta_a \in \mathbb{D}^c_-$. The trajectories associated with the Poincarè half-maps $\check{\mathcal{P}}_{a,b}$ are specified below, and their combination gives rise to the first recurrence map, termed the generalized Poincarè map $\check{\mathcal{P}}$ of the whole system (3.1).

$$\begin{aligned} \check{\mathcal{P}}_a :& \mathbb{D}^c_- \to \mathbb{D}^c_+ \\ & \eta_0 \to \eta_b := \eta(t_a), \\ \check{\mathcal{P}}_b :& \mathbb{D}^c_+ \to \mathbb{D}^c_- \\ & \eta_b \to \eta_a := \eta(\eta(t_a), t_b), \\ \check{\mathcal{P}}(\eta) :=& \check{\mathcal{P}}_b(\check{\mathcal{P}}_a(\eta)). \end{aligned} \tag{3.4}$$

The existence and computation of the return intersection times are indeed challenging, as they remain unknown a priori and are implicitly characterized as nonlinear functions of η.

$$t_r(\eta) := \inf\{t > 0 \mid e_1^T \eta_r(t(\eta), \eta_0) = 0\}, r = a, b. \tag{3.5}$$

The essential criterion for the existence of an invariant half-line on $\mathbb{D}$ that characterizes a periodic orbit is the equation $\check{\mathcal{P}}(\eta) = \eta$, which implies the existence of the quantities η, t_a, t_b. The identification of periodic orbits for the system (3.1) using Poincarè mapping notation requires the application of a root-finding algorithm [30] to resolve the subsequent nonlinear algebraic equations

$$0 = S(X) = \begin{pmatrix} \check{\mathcal{P}}(\eta) - \eta \\ e_1^T \check{\mathcal{P}}_a(\eta) \\ e_1^T \check{\mathcal{P}}_b(\eta) \\ \eta^T \eta - 1 \end{pmatrix}, \tag{3.6}$$

where $X = (\eta, t_a, t_b, a)^T$ are six independent variables, the fourth equation is a normalization condition. If the Jacobian matrix is nonsingular at a particular solution X_0, it follows that the nonlinear system can be addressed through a Newton method as follows:

$$DS\,\Delta X^n = -S(X^n), \quad X^{n+1} = X^n + \Delta X^n. \tag{3.7}$$

For example, assume that the initial guess for the Newton method is : $\eta_0 = (0, -1.0, 1.0)^T \in \mathbb{D}^c_-$. This technique computes the fixed point of the Poincarè mapping at $\eta = (0, 1.1970, -0.8483)^T$, $t_a = 5.7313$, $t_b = 6.4437$, and $a = 1.9$; see Figure 2(a). Moreover, diverse strategies related to the continuation algorithm can be employed to examine families of periodic orbits as they vary with a system parameter.

The Lyapunov exponents of a nonlinear system characterize the convergence and divergence of its states. The presence of a positive Lyapunov exponent indicates that the system exhibits chaotic behavior. The Lyapunov exponents as a function of the varying parameter a are shown in Figure 1(a) for the dynamic system (3.1), with the initial condition $(6.32, 1, -1)$ and the time interval $t \in [0, 200]$.

For example, it has been observed that the Lyapunov characteristic exponents of the Jerk system (3.1) are estimated to be $L_1 = 0.3645$, $L_2 = 0.00005$, and $L_3 = -1.8651$. The Kaplan-Yorke dimension is obtained as:

$$D_{KY} = 2 + \frac{L_1 + L_2}{|L_3|} = 2.1957.$$

This result supports the hypothesis that the Jerk system described in Eq (3.1) is chaotic, as indicated by the presence of one positive Lyapunov exponent.

In addition, the bifurcation diagram, a critical tool in nonlinear theory, is used to numerically investigate the dynamic behavior of the system. This exploration is carried out using a fourth-order Runge-Kutta algorithm, which is supported by a robust event detection method that reliably computes the switching points. In Figure 1(b), the bifurcation diagrams of the variable z versus the parameter a. In more detail, as the value of a decreases from $a = 1.9$, the system transitions from a steady state of period-1 (illustrated in Figure 2(a)) to a scenario of period doubling (depicted in Figure 2(b)), subsequently leading to a chaotic state, as evidenced by the chaotic attractor presented in a three-dimensional space in Figure 2(c).

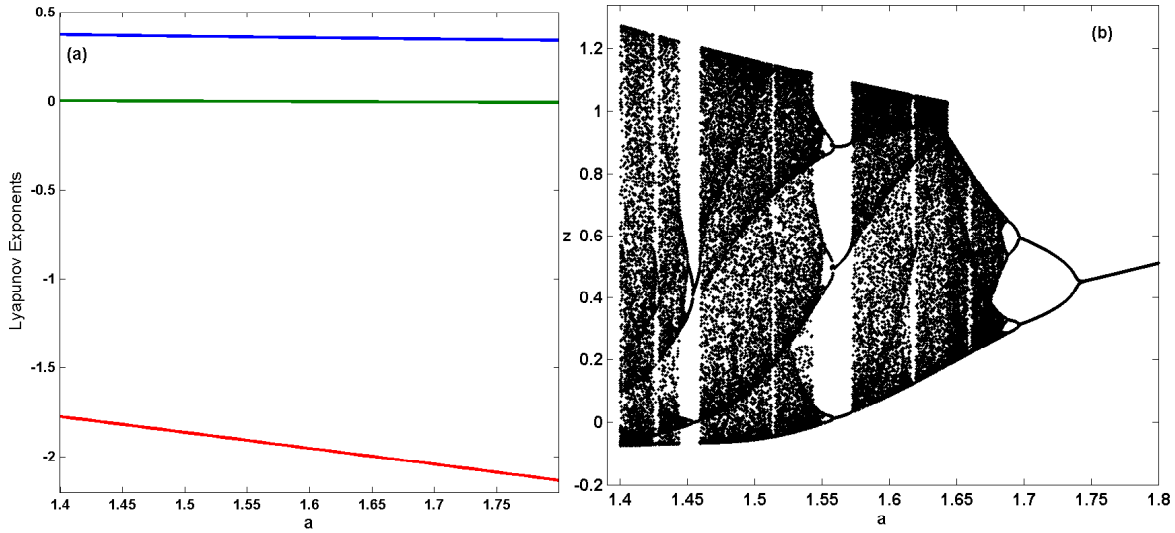

Figure 1. Global dynamics for the system described by (2.6), where the functions are defined as $G_a(\eta) = G_b = -x$. (a) Dynamics of the Lyapunov exponents with respect to variations in the control parameter a. (b) The bifurcation diagram in the $(z - a)$-plane of self-excited attractors, illustrating the path towards chaotic behavior.

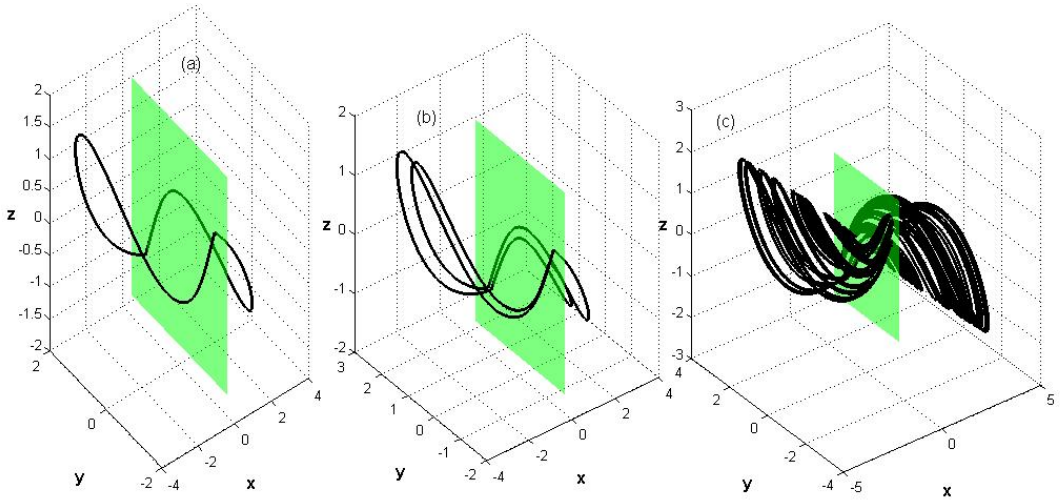

Figure 2. Self-excited attractors are generated on the basis of the existence of equilibria, where $G_a(\eta) = G_b = -x$. (a) Single periodic orbit with a=1.9 and $\eta_0 = (0, 1.1970, -0.8483)$. (b) Period-doubling orbit, with a=1.7 and $\eta_0 = (0, -1.1049, 0.3182)$. (c) Chaotic behavior, with a=1.5 and $\eta_0 = (0, 0.9739, -0.1388)$.

3.2. Case II: $\bar{\eta} = \vec{0} \in \mathbb{D}_b^c$, and $G_a(\bar{\eta}) \neq 0$, $G_b(\bar{\eta}) = 0$

In this context, we characterize the unknown functions present in the system represented by (2.6) as follows:

$$\dot{\eta} = \begin{cases} \mathbb{J}_a(\eta) = \begin{pmatrix} y \\ z \\ -az - y^2 + a - y \end{pmatrix}, & x < 0; \\ \mathbb{J}_b(\eta) = \begin{pmatrix} y \\ z \\ -az + y^2 - x \end{pmatrix}, & x \geqslant 0. \end{cases} \tag{3.8}$$

It is clear that the first subsystem of (3.8) does not have an equilibrium point (that is, when $x < 0$), while the origin appears to be a unique equilibrium point within the second subsystem (that is, when $x \geqslant 0$). In addition, at $\eta_0 \in \mathbb{D}$, a direct crossing region arises because both subsystems exhibit the same value at η_0; that is, $\nabla\hbar(\eta_0))^T\mathbb{J}_a(\eta_0) = \nabla\hbar(\eta_0))^T\mathbb{J}_b(\eta_0) = y_0$. Note that the explicit solution $\eta_b(t)$ is given by (3.3) when $x \geqslant 0$. However, the second subsystem of (3.8) is rewritten as

$$\dot{\eta}_a = \mathbb{J}_a = \bar{A}\eta + (a - y^2)e_3, \quad x < 0, \tag{3.9}$$

where the matrix $\bar{A}$ possesses the eigenvalues given by $\lambda_1 = 0$, $\lambda_{2,3} = \frac{1}{2}\left(-a + \sqrt{a^2 - 4}\right)$, with the associated eigenvectors $V_1 = (1, 0, 0)^T$, $V_2 = \left(\frac{\lambda_2}{\lambda_3}, \lambda_2, 1\right)^T$, and $V_3 = \left(\lambda_3/\lambda_2, \lambda_3, 1\right)^T$. We observe that the eigenvalue $\lambda_1 = 0$ is relevant to the x-axis direction ($x < 0$) in the dynamic system (3.9).

This implies that perturbations along the x-axis remain unchanged in terms of exponential growth or decay, whereas perturbations in the y- and z-directions are pivotal in shaping the system's behavior. The discriminant $a^2 - 4$ contributes to our understanding of the behavior of the subsystem indicated in (3.9). We are particularly concerned with the scenario in which $a^2 < 4$, since this leads to complex eigenvalues and enables the system to display oscillatory behavior in proximity to the discontinuity surface. These eigenvalues and eigenvectors are utilized to derive the analytical solution of the linear system $\dot{\bar{\eta}}_a = \bar{A}\bar{\eta}$, enabling us to obtain the explicit solution for the nonlinear system (3.8). The solution $\bar{\eta_a}(t)$ under the initial condition $\eta_0 = (0, y_0, z_0)^T \in \mathbb{D}$ is given by

$$\bar{\eta}_a(t) = \begin{pmatrix} e^{\alpha t}\left(-C_1\cos(\beta t) - \frac{aC_1-2y_0}{2\beta}\sin(\beta t)\right) + C_1 \\ e^{\alpha\, t}\left(\frac{C_1+z_0}{2\beta}\sin(\beta\, t) + y_0\cos(\beta\, t)\right) \\ e^{\alpha\, t}\left(-\frac{az_0+2y_0}{2\beta}\sin(\beta\, t) + z_0\cos(\beta\, t)\right) \end{pmatrix}, \tag{3.10}$$

where $\alpha = -\frac{a}{2}$, $\beta = \frac{\sqrt{4-a^2}}{2}$, and $C_1 = ay_0 + z_0$.

Assume that the flow represented by the earlier solution is redefined as $\bar{\eta}_a(t) = \phi(\eta_0, t)$. Hence, the general solution of the nonlinear system (3.9) is expressed as follows:

$$\check{\mathcal{P}}_a = \bar{\eta}_a(t) + \int_0^t \bar{\eta}_a(t-s)(a - y(s)^2)e_3\, ds. \tag{3.11}$$

The transition time t_a is determined through numerical methods by solving the equation

$$e_1^T\ \check{\mathcal{P}}_a(\eta) = 0 \tag{3.12}$$

As an example, one can utilize the technique established in Eqs (3.4), (3.6), and (3.7) to compute the transition times and the fixed point that results in a periodic orbit. According to the findings derived from Newton's method, the values are $t_a = 1.9925$, $t_b = 7.649$, $\eta_0 = (0, 0.8485, 0.5544)^T$, and $a = 1.85$. Figure 3(a) demonstrates the periodic orbit of the system outlined in the Eq (3.8), as derived from these results. Figures 3(a), (b), (c), and (d) depict the system transitioning from a period-1 steady state to a chaotic state.

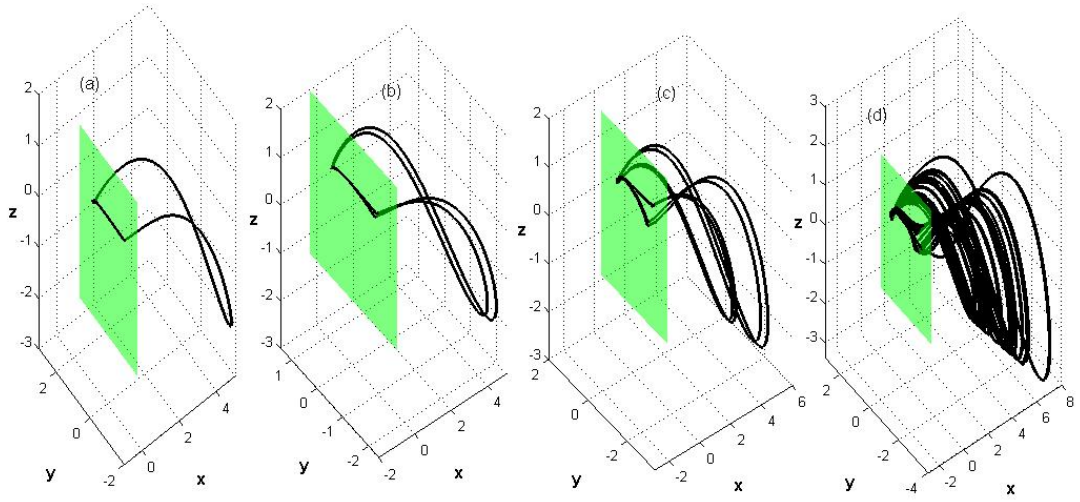

Figure 3. Hidden attractors are generated based on the absence of equilibrium points in one of the subsystems, where $G_a(\eta) = a - y, G_b = -x$, showing a path to chaos. (a) With $a = 1.85$ and $\eta_0 = (0, 0.8485, 0.5544)$; (b) with $a = 1.8$, and $\eta_0 = (0, 0.8429, 0.5576)$; (c) with $a = 1.7$ and $\eta_0 = (0, 0.8605, 0.5294)$; (d) with $a = 1.6$ and $\eta_0 = (0, 0.8897, 0.4378)$.

In order to achieve chaotic behavior, it is essential that the solution to the initial value problem (3.8), $\eta_0 \in \mathbb{D}^c$, exhibits oscillatory characteristics determined by the eigenvalues. The parameter range $0 < a < 2$ ensures that the solution sets for both subsystems are oscillatory in nature, a consequence of having two pairs of complex-conjugate eigenvalues.

The dynamical behavior of the system (3.8) is analyzed using bifurcation diagrams and Lyapunov exponents. For the values of the chosen parameters $a = 1.6$ and $\eta_0 = (0, -1.7031, 2.0477)^T$, the Lyapunov exponents of the chaotic system (3.8) are obtained as follows : $L_1 = 0.3527$, $L_2 \approx 0$, and $L_3 = -1.9527$. The negative sum of L_i for $i = 1, 2, 3$ confirms that the novel system defined by (3.8) has dissipative properties. The Kaplan–Yorke dimension is calculated as

$$D_{KY} = 2 + \frac{L_1 + L_2}{|L_3|} = 2.1806.$$

The Lyapunov exponents as a function of the varying parameter a are illustrated in Figure 4 (left). The bifurcation diagram is also obtained for the range $1.55 \leqslant a \leqslant 1.85$, and is shown in Figure 4 (right). The system is demonstrated to transition into chaos via a series of period doublings, confirming the presence of chaos; see Figure 4.

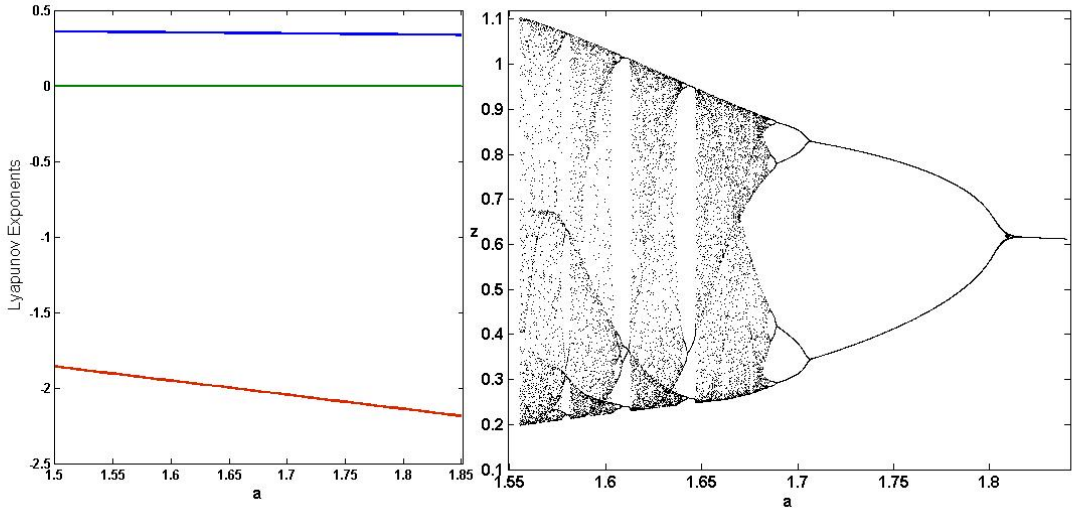

Figure 4. Global dynamics for the system described by (3.8), indicating a path to chaos. (left) Dynamics of the LEs with respect to variations of a. (right) A bifurcation diagram of for z versus a.

3.3. Case III: $\bar{\eta} = \vec{0} \in \mathbb{D}$ and $G_a(\bar{\eta}) \neq G_b(\bar{\eta}) \neq 0$

This section investigates the dynamic behavior that occurs when neither subsystem in (2.6) has any equilibrium points. It is worth noting that the study in [34] examined a discontinuous linear planar system separated by a nonregular line and proved that piecewise-linear systems without equilibria can exhibit limit cycles. These results indicate that the discontinuous system can exhibit unique behavior compared with continuous systems.

The unknown system functions $G_a(\eta)$ and $G_b(\eta)$ are illustrated in the following discontinuous system as follows:

$$\dot{\eta} = \begin{cases} \mathbb{J}_a(\eta) = \begin{pmatrix} y \\ z \\ -az - y^2 + a - y \end{pmatrix}, & x < 0; \\ \mathbb{J}_b(\eta) = \begin{pmatrix} y \\ z \\ -az + y^2 - (1 + xz) \end{pmatrix}, & x \geqslant 0. \end{cases} \tag{3.13}$$

It is obvious that there are no equilibrium points in both vector fields. Traditional methods of stability analysis, such as linearization around fixed points, cannot be used directly because neither region has any equilibrium points. Nonetheless, we can analyze the overall flow characteristics to better understand the system's behavior. At $\eta_0 \in \mathbb{D}$, (i.e., $x = 0$), it is evident that the system transitions between $\mathbb{J}_a(\eta)$ and $\mathbb{J}_b(\eta)$, with the behaviour near this boundary being dictated by the trajectory that approaches it.

- If $x \to 0^-$, the dynamics are governed by $\mathbb{J}_a(\eta)$

$$\mathbb{J}_a(\eta) = \begin{pmatrix} y \\ z \\ -az - y^2 + a - y \end{pmatrix}.$$

- If $x \to 0^+$, the dynamics are governed by $\mathbb{J}_b(\eta)$

$$\mathbb{J}_b(\eta) = \begin{pmatrix} y \\ z \\ -az + y^2 - (1 + xy) \end{pmatrix}.$$

The discontinuities in $\dot{z}$ at $x = 0$ can cause abrupt changes in the system's trajectory. This behavior introduces complex switching dynamics, which depend on the trajectory's direction and velocity as it crosses the boundary $x = 0$. The bifurcation diagram and the Lyapunov exponent spectrum are employed to analyze the discontinuous system (3.13) as a function of its control parameter to establish the type of scenario that produces complex dynamics. When we set $a = 0.77$ and the initial conditions $(0.0, -1.7031, 2.0477)$, the Lyapunov exponents are calculated as: $L_1 = 0.4165, L_2 \approx 0, L_3 = -1.1865$, and the Kaplan-Yorke dimension in the 3D case is calculated to be:

$$D_{KY} = 2 + \frac{L_1 + L_2}{|L_3|} = 2.3511.$$

The dynamics of the Lyapunov exponents are shown in Figure 5 (left). We also observe a cascade of period doubling through the bifurcation diagram (Figure 5 (right)).

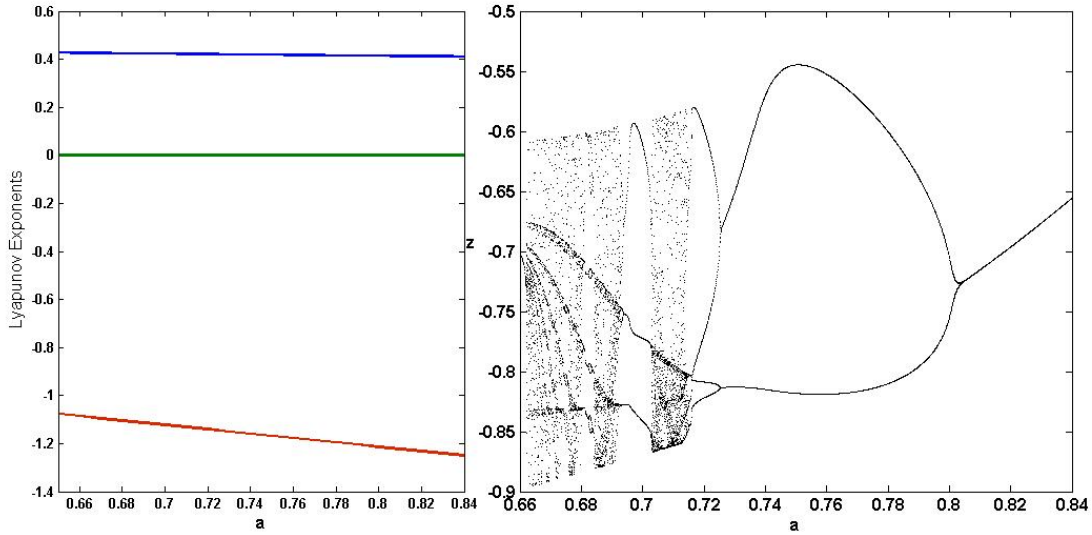

Figure 5. Global dynamics for the system described by (3.13), indicating a path to chaos. Dynamics of the LEs versus a (left). A bifurcation diagram for z versus a (right).

4. Hidden attractors with sliding mode

The trajectories of the dynamical systems (3.1), (3.8), and (3.13) do not involve the sliding mode. We are redefining the discontinuity surface as $\mathbb{D} = \{X \in \mathbb{U} \mid \hbar(\eta) = x+z = 0\}$. Thus, the discontinuous system indicated in (3.13) is revised to

$$\dot{\eta} = \begin{cases} \mathbb{J}_a(\eta) = \begin{pmatrix} y \\ z \\ -az - y^2 + a - y \end{pmatrix}, & x + z < 0, \\ \mathbb{J}_b(\eta) = \begin{pmatrix} y \\ z \\ -az + y^2 - (1 + xz) \end{pmatrix}, & x + z > 0. \end{cases} \tag{4.1}$$

Since $\hbar(\eta) = x + z$, then $\sigma_a = a(1 - z) - y^2$ and $\sigma_b = (y + 0.5)^2 + (z - 0.5a)^2 - \frac{a^2+5}{4}$. Therefore, the discontinuity set is divided into separate regions. The crossing and sliding regions are given as follows:

$$\mathbb{D}^c_- := \left\{ \eta \in \mathbb{R}^3 \mid a(1 - z) < y^2, \ (y + 0.5)^2 + (z - 0.5a)^2 < \frac{a^2 + 5}{4} \right\},$$

$$\mathbb{D}^c_+ := \left\{ \eta \in \mathbb{R}^3 \mid a(1 - z) > y^2, \ (y + 0.5)^2 + (z - 0.5a)^2 > \frac{a^2 + 5}{4} \right\},$$

$$\mathbb{D}^s_a := \left\{ \eta \in \mathbb{R}^3 \mid a(1 - z) > y^2, \ (y + 0.5)^2 + (z - 0.5a)^2 < \frac{a^2 + 5}{4} \right\},$$

$$\mathbb{D}^s_r := \left\{ \eta \in \mathbb{R}^3 \mid a(1 - z) < y^2, \ (y + 0.5)^2 + (z - 0.5a)^2 > \frac{a^2 + 5}{4} \right\}.$$

Figure 6(a) depicts the discontinuity surface $\hbar(\eta)$, which is divided into the crossing and sliding regions.

Here, we focus on the case when the orbit of (4.1) gets close to an attracting sliding region $\mathbb{D}^s_a$, where it may come into interactions with the sliding surface and slide along it. The Fillipov extension describes the behavior of sliding motion in the following way:

$$\dot{\eta} = F_s(\eta) = S_a(\eta)\mathbb{J}_a(\eta) + S_b(\eta)\mathbb{J}_b(\eta), \quad \eta \in \mathbb{D}, \tag{4.2}$$

where $S_a(\eta) = -\frac{(y+0.5)^2+(z-0.5a)^2-\frac{a^2+5}{4}}{a+1-\left(z^2+y(2y+1)\right)}$ and $S_b(\eta) = \frac{a(1-z)-y^2}{a+1-\left(z^2+y(2y+1)\right)}$, and the system (4.2) is reduced to system of linear ordinary differential equations as follows:

$$\dot{\eta} = F_s(\eta) = \begin{pmatrix} y \\ z \\ -y \end{pmatrix}, \quad \eta \in \mathbb{D}, \tag{4.3}$$

Within this sliding flow, there is a pseudo-equilibrium point located at the origin that serves as the center point. The eigenvalues of the Jacobian matrix for the linear system (4.3) are $\lambda_1 = 0$ and $\lambda_{2,3} = \pm i$, which supports this characterization. In addition, the sliding system (4.3) behaves like a harmonic oscillator, with all variables oscillating in a periodic manner. It should be noted that the presence of a single zero eigenvalue is due to the sliding flow mode's singularity, which restricts its behavior to a two-dimensional domain.

The general solution for the sliding system (4.3), where $\eta_0 \in \mathbb{D}_a^s$, is derived as follows:

$$\begin{aligned} x(t) &= -z_0 \cos(t) + y_0 \sin(t), \\ y(t) &= z_0 \sin(t) + y_0 \cos(t), \\ z(t) &= z_0 \cos(t) - y_0 \sin(t). \end{aligned} \tag{4.4}$$

Assuming $\eta_0 \in \mathbb{D}_a^s$, the sliding flow has two possible behaviours. In one case, the flow continues indefinitely within the sliding region, whereas in the other, the flow eventually reaches one of the boundaries. Solving one of the following equations yields the duration required for the flow of the sliding system to reach one of the boundaries $\sigma_a = 0$ or $\sigma_b = 0$.

$$E_1 = a\left(z_0 \cos(t) - y_0 \sin(t)\right) + \left(z_0 \sin(t) + y_0 \cos(t)\right)^2 - a = 0,$$

$$E_2 = \left(z_0 \sin(t) + y_0 \cos(t) + 0.5\right)^2 + \left(z_0 \cos(t) - y_0 \sin(t) - 0.5a\right)^2 - \frac{a^2+5}{4} = 0.$$

Consider the scenario where $\eta \in \mathbb{D}_a^s$ and the flow progresses towards the boundary $\sigma_a = 0$. The sliding time flow represents the first positive zero of the function E_1, as shown in Figure 6(b), as the parameter a changes.

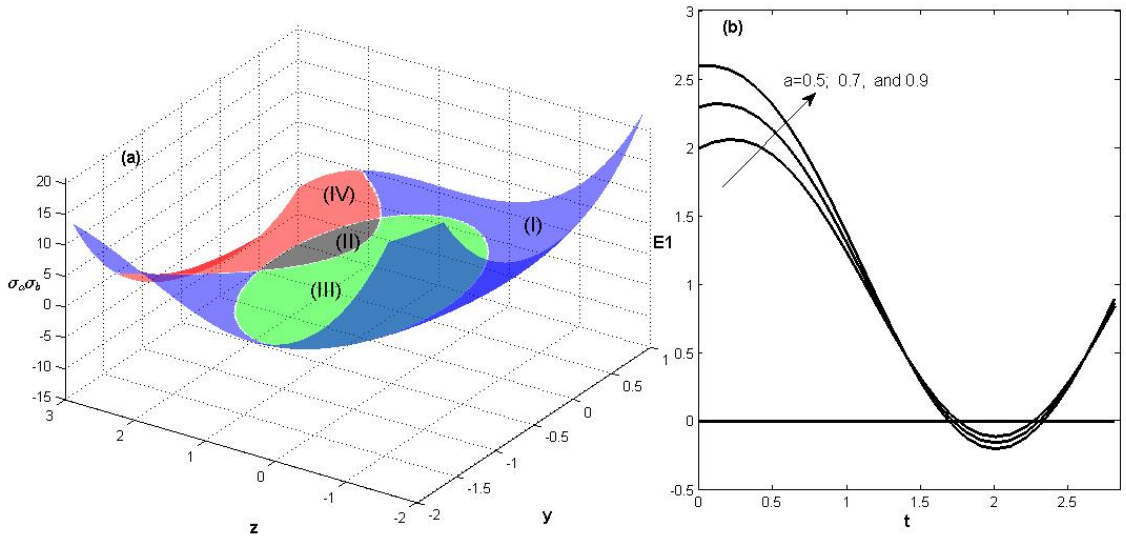

Figure 6. (a) The numerical computation of the location of crossing and sliding regions on the discontinuity surface. (I) The crossing region $\mathbb{D}_b^c$, (II) the crossing region $\mathbb{D}_a^c$, (II) the crossing region $\mathbb{D}_b^c$, (III) an attracting sliding region $\mathbb{D}_a^s$, and (IV) a repelling sliding region $\mathbb{D}_r^s$. (b) The existence of the sliding flow time, which represents the first zero of the function E_1, as the parameter a changes.

Theorem 1. *Assume that* $\eta_0 = (x_0, 0, z_0)^T \in \mathbb{D}_a^s$ *and* $\frac{a-\sqrt{a^2+4}}{2} < z_0 < 1$. *The dynamics of the Jerk-like system* (4.1)*, separated by the surface* $\hbar = x + z$ *and lacking both real and virtual equilibria, reveal that within the sliding region surrounding the pseudo-equilibrium, a family of periodic orbits exists with the period* $t = 2\pi$.

Proof: The parameter a does not affect the general solution (4.4) of the sliding flow but does affect the identification of the attracting sliding region $\mathbb{D}_a^s$. Since $\eta_0 = (x_0, 0, z_0)^{\in}\mathbb{D}_a^s$, and according to the definition of the attracting sliding region $\mathbb{D}_a^s$ (i.e., $\sigma(\eta_0) > 0$, and $\sigma_b(\eta_0) < 0$), it follows that $\frac{a-\sqrt{a^2+4}}{2} < z_0 < 1$.

We define the Poincarè map associated with the sliding flow (4.3) using the general solution (4.4), which is $\check{\mathcal{P}}_s(\eta) :== \mathbb{D}_a^s \to \mathbb{D}_a^s$. The sliding flow is linear in η and homogeneous, allowing it to maintain linear homogeneity, as indicated by $\check{\mathcal{P}}_s(m\eta) = m\check{\mathcal{P}}(\eta)$ and $\frac{\partial\check{\mathcal{P}}}{\partial\eta}(m\eta) = \frac{\partial\check{\mathcal{P}}}{\partial\eta}$ for some $m \in R^+$. Evaluating the Poincarè map at the point $\eta_0 = (x_0, 0, z_0)^T \in \mathbb{D}_a^s$ results in $t = 2\pi$ and $\check{\mathcal{P}}_s(m\eta_0) = m\eta_0$. As a consequence, the sliding flow has a family of flat periodic orbits that occur only in the sliding region $\mathbb{D}_a^s$. Figure 7 depicts a family of periodic orbits that are exclusively in sliding mode, with $a = 0.9$ and $a = 0.3$.

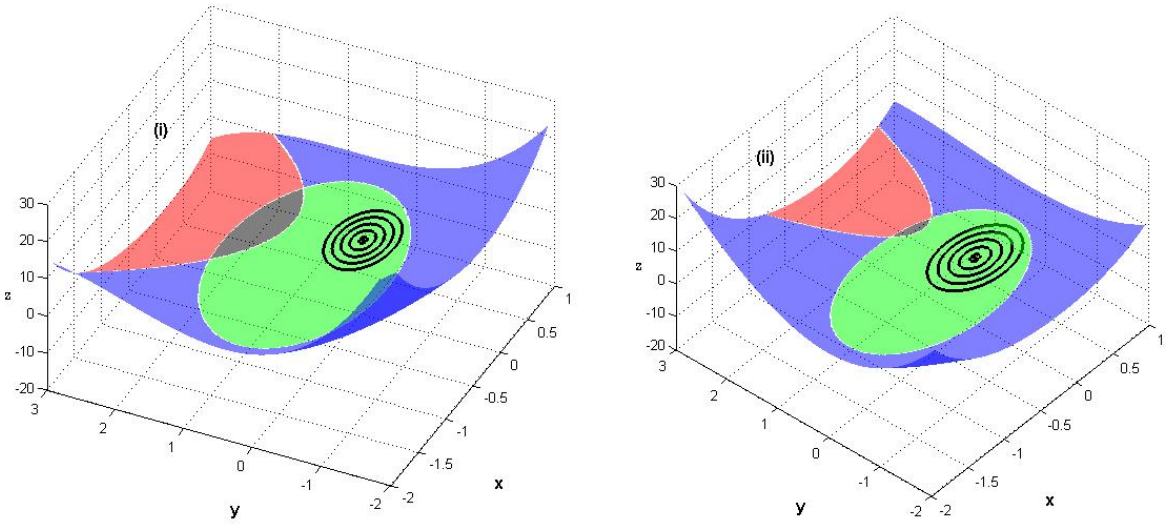

Figure 7. A family of periodic orbits that are exclusively in sliding mode. (I) $a = 0.9$ and (II) $a = 0.3$.

Figure 8(a) and (b) highlights that the Jerk-like system (4.1) without equilibria establishes a single periodic orbit with a sliding mode at $a = 0.9$ and $\eta_0 = (0.2653, 0.8251, -0.2653)^T$. Figure 8(c) and (d) highlights that when the parameter a is varied (that is, $a = 0.83$), a period-doubling orbit appears with a sliding segment, with the initial condition set as $\eta_0 = (0.3473, 0.7280, -0.3473)^T$. Figure 9 shows a specific transition of behavior, including a sliding mode from the period-k orbit ($k \in R$) to chaos, which is detected by varying the parameter a. The Jerk-like system (4.1) exhibits a period-k orbit at $a = 0.8$ with $\eta_0 = (0.5829, -0.5083, -0.5829)^T \in \mathbb{D}_a^s$ and chaotic behavior at $a = 0.75$ with $\eta_0 = (0.5208, -0.6836, -0.5208)^T \in \mathbb{D}_a^s$, as shown in Figure 9(a) and (b) and Figure 9(c) and (d),

respectively.

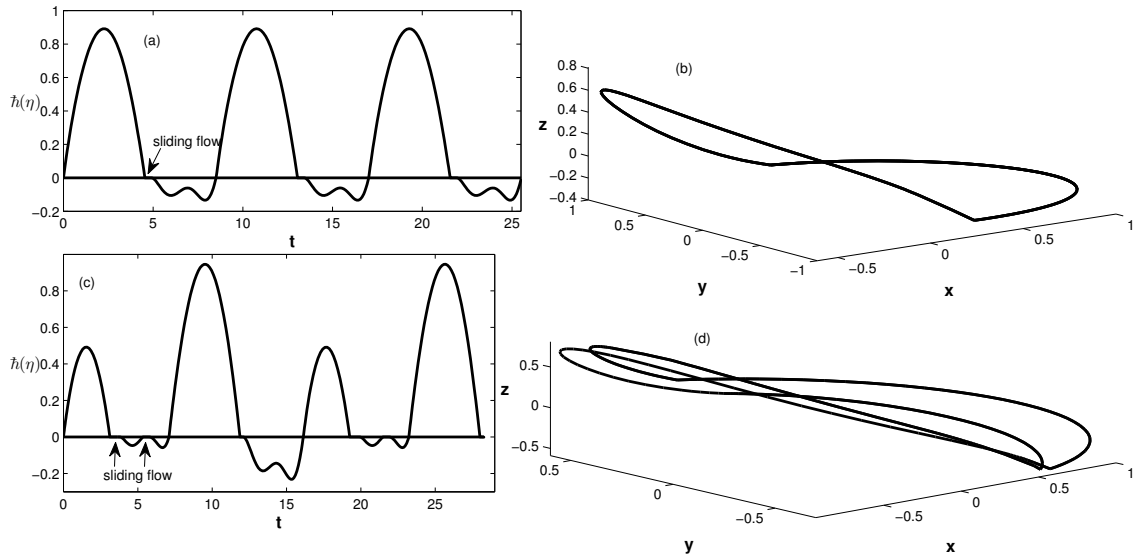

Figure 8. The Jerk-like system (4.1) without equilibria recognizes various dynamic behaviors, including the sliding mode, where (a) and (b) illustrate the existence of a unique periodic orbit at $a = 0.9$, where (c) and (d) illustrate the existence of a period-doubling orbit at $a = 0.83$.

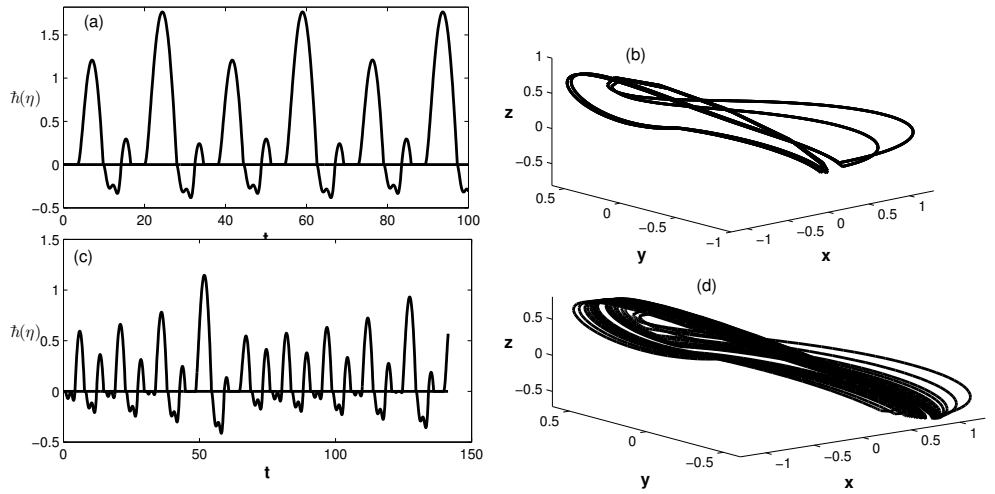

Figure 9. The Jerk-like system (4.1) without equilibria recognizes various dynamic behaviors, including the sliding mode, where (a) and (b) illustrate the existence of a unique periodic orbit at $a = 0.9$, and (c) and (d) illustrate the existence of a period-doubling orbit at $a = 0.83$.

5. Conclusions

We present a novel chaotic Jerk-like system distinguished by discontinuous vector fields separated by a codimension-1 switching surface $\mathbb{D}$. A qualitative investigation was conducted on the proposed discontinuous systems generated from dissipative subsystems, both with and without equilibria. The study focused on the nonsmooth bifurcation characteristics of the switching surface $\mathbb{D}$, where orbits may either cross or exhibit sliding behavior. While the new system may have equilibrium and nonequilibrium points, it generates periodic orbits, period-doubling, and chaotic dynamics that include both self-excited and hidden attractors. In particular, the intersection of attractors and sliding modes has been observed to exhibit an unusual phenomenon, resulting in the formation of a family of periodic orbits within the sliding region that surrounds the pseudo-equilibrium. The dynamic properties of the proposed system, both self-excited and hidden attractors, are confirmed by using phase portraits, geometric analysis, Poincaré maps, bifurcation diagrams, and Lyapunov exponents. Further analysis or numerical simulations are required to fully understand the impact of this switching on the system's overall behavior.

The Jerk systems with discontinuities exhibit sliding motion, a phenomenon in which trajectories slide over $\mathbb{D}$. This sliding characteristic is particularly useful in control systems, mechanical systems with impacts, and electrical circuits with switching components. This paves the way for practical applications, including the development of robust sliding mode controllers, vibration isolation systems, and nonlinear oscillators for signal generation. Future research may benefit from employing continuation methods to obtain quantitative characterizations of the basins of attraction. Furthermore, the proposed system may exhibit various aspects of multistability due to its high sensitivity to the initial conditions and abrupt changes in behavior caused by the inequality of the Jacobians on either side of the discontinuity surface. This has motivated us to continue developing an accurate algorithm for efficiently managing the root identifying of the event function $\hbar(\eta)$ in discontinuous Jerk systems (2.6) with multiple abrupt changes and recurrent reordering for the variational Eq (2.5).

Use of Generative-AI tools declaration

The author declares that he has not used Artificial Intelligence (AI) tools in the creation of this article.

Acknowledgments

The author is thankful to the Deanship of Graduate Studies and Scientific Research at the University of Bisha for supporting this work through the Fast-Track Research Support Program.

Conflict of interest

The author declares no conflict of interest in this paper.

References

1. E. N. Lorenz, Deterministic nonperiodic flow, *J. Atmos. Sci.*, **20** (1963), 130–141. https://doi.org/10.1175/1520-0469(1963)020¡0130:dnf¿2.0.co;2
2. S. Mangiarotti, M. Peyre, Y. Zhang, M. Huc, F. Roger, Y. Kerr, Chaos theory applied to the outbreak of Covid-19: An ancillary approach to decision-making in pandemic context, *Epidemiol. Infect.*, **148** (2020), e95. https://doi.org/10.1017/S0950268820000990
3. F. Scheck, *Mechanics: from Newton's laws to deterministic chaos*, 5 Eds., Heidelberg: Springer, 2010. https://doi.org/10.1007/978-3-642-05370-2
4. D. Toker, F. T. Sommer, M. D'Esposito, A simple method for detecting chaos in nature, *Commun. Biol.*, **3** (2020), 11. https://doi.org/10.1038/s42003-019-0715-9
5. C. K. Volos, I. M. Kyprianidis, I. N. Stouboulos, Experimental demonstration of a chaotic cryptographic scheme, *WSEAS Transactions on Circuits and Systems Archive*, **5** (2006), 1654–1661.
6. A. A. Zaher, A. Abu-Rezq, On the design of chaos-based secure communication systems, *Commun. Nonlinear Sci.*, **16** (2011), 3721–3737. https://doi.org/10.1016/j.cnsns.2010.12.032
7. N. V. Kuznetsov, G. A. Leonov, V. I. Vagaitsev, Analytical-numerical method for attractor localization of generalized Chua's system, *IFAC Proceedings Volumes*, **43** (2010), 29–33. https://doi.org/10.3182/20100826-3-tr-4016.00009 .
8. G. A. Leonov, N. V. Kuznetsov, V. I. Vagaitsev, Localization of hidden Chua's attractors, *Phys. Lett. A*, **375** (2011), 2230–2233. https://doi.org/10.1016/j.physleta.2011.04.037
9. G. A. Leono, N. V. Kuznetsov, Hidden attractors in dynamical systems: From hidden oscillations in hilbert-kolmogorov, Aizerman, and Kalman problems to hidden chaotic attractor in Chua circuits, *Int. J. Bifurcat. Chaos*, **23** (2013), 1330002. https://doi.org/10.1142/S0218127413300024
10. H. A. Hosham, M. A. Aljohani, E. D. A. Elela, N. A. Almuallem, T. N. Alharthi, Hidden-like attractors in a class of discontinuous dynamical systems, *Mathematics*, **12** (2024), 3784. https://doi.org/10.3390/math12233784
11. S. Garai, S. Karmakar, S. Jafari, N. Pal, Coexistence of triple, quadruple attractors and Wada basin boundaries in a predator–prey model with additional food for predators, *Commun. Nonlinear Sci.*, **121** (2023), 107208. https://doi.org/10.1016/j.cnsns.2023.107208
12. A. Dhooge, W. Govaerts, Y. A. Kuznetsov, MATCONT: A MATLAB package for numerical bifurcation analysis of ODEs. *ACM T. Math. Software*, **29** (2003), 141–164. https://doi.org/10.1145/779359.779362
13. J. Lebl, Ordinary differential equations, In: *Computational toxicology*, Totowa: Humana Press, 2013, 475–498. https://doi.org/10.1007/978-1-62703-059-5_20
14. R. H. Clewley, W. E. Sherwood, M. D. LaMar, J. M. Guckenheimer, PyDSTool, a software environment fo dynamical systems modeling, 2007. Available from: `http://pydstool.sourceforge.net`

15. V. Rybin, D. Butusov, K. Shirnin, V. Ostrovskii, Revealing hidden features of chaotic systems using high-performance bifurcation analysis tools based on cuda technology, *Int. J. Bifurcat. Chaos*, **34** (2024), 2450134. https://doi.org/10.1142/S0218127424501347

16. D. Dantsev, A novel type of chaotic attractor for quadratic systems without equilibriums, *Int. J. Bifurcat. Chaos*, **28** (2018), 1850001. https://doi.org/10.1142/S0218127418500013

17. A. P. Kuznetsov, S. P. Kuznetsov, E. Mosekilde, N. V. Stankevich, Co-existing hidden attractors in a radio-physical oscillator system, *J. Phys. A: Math. Theor.*, **48** (2015), 125101. https://doi.org/10.1088/1751-8113/48/12/125101

18. S. N. Chowdhury, D. Ghosh, Hidden attractors: A new chaotic system without equilibria, *Eur. Phys. J. Spec. Top.*, **229** (2020), 1299–1308. https://doi.org/10.1140/epjst/e2020-900166-7

19. J. P. Singh, V. T. Pham, T. Hayat, S. Jafari, F. E. Alsaadi, B. K. Roy, A new four-dimensional hyperjerk system with stable equilibrium point, circuit implementation, and its synchronization by using an adaptive integrator backstepping control, *Chinese Phys. B*, **27** (2018), 100501. https://doi.org/10.1088/1674-1056/27/10/100501

20. X. Wang, A. Akgul, S. Cicek, V. T. Pham, D. V. Hoang, A Chaotic system with two stable equilibrium points: dynamics, circuit realization and communication application, *Int. J. Bifurcat. Chaos*, **27** (2017), 1750130. https://doi.org/10.1142/S0218127417501309

21. X. Wang, N. V. Kuznetsov, G. R. Chen, *Chaotic systems with multistability and hidden attractors*, Cham: Springer, 2021. https://doi.org/10.1007/978-3-030-75821-9

22. P. C. Rech, Self-excited and hidden attractors in a multistable jerk system, *Chaos Soliton. Fract.*, **164**, (2022), 112614. https://doi.org/10.1016/j.chaos.2022.112614

23. X. Y. Hu, B. Sang, N. Wang, The chaotic mechanisms in some jerk systems, *AIMS Mathematics*, **7** (2022), 15714–15740. https://doi.org/10.3934/math.2022861

24. H. A. Hosham, Nonlinear behavior of a novel switching jerk system, *Int. J. Bifurcat. Chaos*, **30** (2020), 2050202. https://doi.org/10.1142/S0218127420502028

25. J. C. Sprott, Some simple chaotic jerk functions, *Am. J. Phys.*, **65** (1997), 537–543. https://doi.org/10.1119/1.18585

26. J. C. Sprott, A new class of chaotic circuit, *Phys. Lett. A*, **266** (2000), 19–23. https://doi.org/10.1016/S0375-9601(00)00026-8

27. J. X. Zhang, G. D. Li, H. P. Pan, X. K. Chen, Multi-scroll expansion of 3D and 4D Jerk systems and its DSP implement, *Chinese J. Phys.*, **94** (2025), 627–649. https://doi.org/10.1016/j.cjph.2025.02.002

28. S. J. Linz, J. C. Sprott, Elementary chaotic flow, *Phys. Lett. A*, **259** (1999), 240–245. https://doi.org/10.1016/S0375-9601(99)00450-8

29. J. Awrejcewicz, C.-H. Lamarque, *Bifurcation and chaos in nonsmooth mechanical systems*, Singapore: World Scientific, 2003. https://doi.org/10.1142/5342

30. T. Küpper, H. A. Hosham, Reduction to invariant cones for non-smooth systems, *Math. Comput. Simulat.*, **81** (2011), 980–995. https://doi.org/10.1016/j.matcom.2010.10.004

31. W. K. Zhou, T. T. Zhao, A. L. Wang, S. Y. Tang, Bifurcations and dynamics of a filippov epidemic model with nonlinear threshold control policy and medical-resource constraints, *Chaos Soliton. Fract.*, **184** (2024), 114992. https://doi.org/10.1016/j.chaos.2024.114992

32. M. Messias, R. P. Silva, Determination of nonchaotic behavior for some classes of polynomial Jerk equations. *Int. J. Bifurcat. Chaos*, **30** (2020), 2050117. https://doi.org/10.1142/S0218127420501175

33. J. R. M. Pone, V. K. Tamba, G. H. Kom, A. B. Tiedeu, Period-doubling route to chaos, bistability and antimononicity in a jerk circuit with quintic nonlinearity, *Int. J. Dynam. Control*, **7** (2019), 1–22. https://doi.org/10.1007/s40435-018-0431-1

34. Z. K. Li, X. B. Liu, Limit cycles in discontinuous piecewise Linear planar Hamiltonian systems without equilibrium points, *Int. J. Bifurcat. Chaos*, **32** (2022), 2250153. https://doi.org/10.1142/S021812742250153X

35. H. A. Hosham, T. N. Alharthi, Bifurcation and chaos in simple discontinuous systems separated by a hypersurface, *AIMS Mathematics*, **9** (2024), 17025–17038. https://doi.org/10.3934/math.2024826

36. M. B. Laurea, A. R. Champneys, C. J. Budd, P. Kowalczyk, *Piecewise-smooth dynamical systems: theory and applications*, London: Springer, 2008. https://doi.org/10.1007/978-1-84628-708-4

37. M. Van, Higher-order terminal sliding mode controller for fault accommodation of Lipschitz second-order nonlinear systems using fuzzy neural network, *Appl. Soft Comput.*, **104** (2021), 107186. https://doi.org/10.1016/j.asoc.2021.107186

38. A. F. Filippov, *Differential equations with discontinuous righthand sides: control Systems*, Dordrecht: Springer, 1988. https://doi.org/10.1007/978-94-015-7793-9

39. R. I. Leine, D. H. van Campen, B. L. van de Vrande, Bifurcations in nonlinear discontinuous systems, *Nonlinear Dyn.*, **23** (2000), 105–164. https://doi.org/10.1023/A:1008384928636

40. M. E. Kahoui, A. Weber, Deciding Hopf bifurcations by quantifier elimination in a software-component architecture, *J. Symb. Comput.*, **30** (2000), 161–179. https://doi.org/10.1006/jsco.1999.0353

AIMS Press